Reduction in Northern Midlatitude 2-m Temperature Variability due to Arctic Sea Ice Loss

THOMAS W. COLLOW, WANQIU WANG, AND ARUN KUMAR

NOAA/NWS/NCEP Climate Prediction Center, College Park, Maryland

(Manuscript received 15 October 2018, in final form 13 May 2019)

ABSTRACT

In this study, we investigate links between Arctic sea ice loss and the variability of 2-m temperatures over a 6-month period (November–April) over two domains centered over northern Eurasia and northern North America. Based on data from the Climate Forecast System Reanalysis (CFSR), there has been an increase (a decrease) in recent seasonal temperature variability over Eurasia (North America), which can be attributed to cooling (warming) during the winter months. Decreases in the intraseasonal variability of temperature anomalies, however, are noted in both regions for the November–April period. This study investigates the role of different forcings on the changes seen in the reanalysis product using Atmospheric Model Intercomparison Project simulations forced with repeating sea surface temperature, sea ice, and carbon dioxide concentration relative to climatologies from two different base periods, 1981–90 and 2005–14. The seasonal temperature and intraseasonal anomaly variabilities are examined, and we find that only the simulations with reduction in sea ice (2005–14 base-period sea ice concentration) produce significant decreases in intraseasonal temperature anomaly variability over these regions, agreeing with the CFSR analysis. Runs that reduce sea ice also result in a significant decrease in the frequency and magnitude of extreme warm and cold temperature anomalies. It is proposed that the weakened latitudinal temperature gradient, resulting from decreased sea ice, leads to reduced meridional temperature advection variability, which in turn contributes to the reduction in the variability of temperature anomalies.

1. Introduction

Declining Arctic sea ice and its impacts on midlatitude weather and climate has been a major topic of scientific debate in recent years. Sea ice loss leads to additional Arctic warming through the ice–ocean albedo feedback (Kumar et al. 2010; Screen and Simmonds 2010). Because open water has a lower albedo than sea ice, a region with open water absorbs more solar radiation than ice, thus increasing the temperature further than if the same region were covered by ice. LaJoie and DelSole (2016) show that, in addition to mean warming in the twenty-first century, 2-m temperature variance decreases in seasonal ice marginal zones (regions that experience sea ice melt and refreeze each year) because of the larger heat capacity of newly exposed water. The overarching question is whether sea ice loss and associated Arctic amplification produce only local impacts with a small influence on the global climate or whether they can also trigger atmospheric circulation changes, which can have a larger effect on the global climate.

Francis and Vavrus (2012, 2015) claim that Arctic amplification, by reducing the north–south temperature gradient, weakens the zonal jet stream allowing for more persistent weather patterns and a greater likelihood of extreme events. Other studies have also argued for at least some impact on midlatitude weather from sea ice loss. Examples include decreased temperature variance in the northern midlatitudes (Screen 2014), a more negative phase of the Arctic and North Atlantic Oscillations (Liu et al. 2012; Nakamura et al. 2015; Screen 2017), and an increase in surface atmospheric pressure over Siberia (Honda et al. 2009; Cohen et al. 2012; Inoue et al. 2012; Zhang et al. 2012; Tang et al. 2013; Zappa et al. 2018). Conversely, several studies also suggest no significant attributable linkages between Arctic amplification and midlatitude seasonal climate and argue that internal variability is the dominant factor in recent observed changes (Barnes 2013; Barnes et al. 2014; Screen and Simmonds 2013, Screen et al. 2014; Perlwitz et al. 2015; McCusker et al. 2016; Sun et al. 2016; Collow et al.

Corresponding author: Thomas W. Collow, thomas.collow@noaa.gov

DOI: 10.1175/JCLI-D-18-0692.1

2018; Ogawa et al. 2018). Despite considerable research, however, issues with the use of inconsistent methodologies, differences in dynamical models (and associated simulations), and limited observations make deducing linkages between Arctic sea ice decline and lower-latitude climate variability a challenging task (Cohen et al. 2014).

Following on previous research, this study assesses changes in daily temperature variability in the Climate Forecast System Reanalysis (CFSR; Saha et al. 2010), focusing on the near-surface (2 m above ground) temperature. Atmospheric Model Intercomparison Project (AMIP) simulations using the atmospheric component of the Climate Forecast System, version 2 (CFSv2; Saha et al. 2014), model are then used to attribute the changes in temperature variability to the evolution in different forcings—namely, sea ice cover, sea surface temperatures (SSTs), and carbon dioxide (CO_2) concentration—over the recent decades. Whereas the Collow et al. (2018) study focused on mean temperature changes on a seasonal time scale, this analysis looks into temperature variability within the late autumn and winter seasons, with an emphasis on the northern midlatitudes as these regions have been argued to have a reduction in variability resulting from sea ice loss (Screen 2014; Screen et al. 2015; Blackport and Kushner 2016; 2017). Our study benefits from a systematic use of model sensitivity experiments that can isolate the impacts of sea ice loss, SST increase, and CO_2 concentration increase in recent decades. We aim to address the following questions in the context of AMIP simulations using CFSv2: 1) Can the AMIP simulations represent the observed changes in the variability of northern midlatitude temperatures? 2) How is the overall intraseasonal temperature anomaly distribution affected by the different forcings? 3) Can a physical pathway be established that links the boundary condition perturbations with the changes in temperature variability?

2. Methods

a. Model simulations

The model used for this study is the atmospheric component of CFSv2 (Moorthi et al. 2001), which uses a T126 horizontal grid (approximately 100-km grid spacing) and 64 sigma-pressure hybrid layers, with the top layer being at 1-hPa pressure level. Five sets of simulations are done with repeating annual cycle having combinations of monthly mean sea ice concentration (SIC), SST, and CO_2 concentration boundary conditions for 101 yr. The specified boundary conditions are generated by taking the 10-yr monthly means of SIC and SST data from the merged Hadley–NOAA/optimum interpolation (OI) dataset (Hurrell et al. 2008), and CO_2 data from the NCEP operational archive. Specifically, the combinations used are listed in Table 1 and are the control run, referred to as 8190ALL (SST, SIC, and CO_2 1981–90 mean), 0514SST (SST 2005–14 mean; SIC and CO_2 1981–90 mean), 0514ICE (SIC 2005–14 mean; SST and CO_2 1981–90 mean), 0514CO_2 (CO_2 2005–14 mean; SST and SIC 1981–90 mean), and 0514ALL (SST, SIC, and CO_2 2005–14 mean). The model runs are postprocessed with data output every 12 h on a 1° × 1° latitude/longitude horizontal grid. The same set of simulations was used in Collow et al. (2018).

TABLE 1. Model simulations and initial-condition years used in this study.

Model simulation	SST	SIC	CO_2
8190ALL	1981–90	1981–90	1981–90
0514ALL	2005–14	2005–14	2005–14
0414SST	2005–14	1981–90	1981–90
0514ICE	1981–90	2005–14	1981–90
0514CO2	1981–90	1981–90	2005–14

b. Analysis

For the variables of interest in this study (2-m temperature and 10-m meridional wind), we average the 12-hourly output into a daily mean at each grid point. Then, starting from November of the first year, we group the data into 6-month bins (from November through the following April), and there are 100 total groupings (or samples) of daily data from the beginning of November to the end of the following April. This procedure is repeated for the five simulations with different configurations of boundary conditions.

We analyze two parameters in this study. The first is of the seasonal cycle of 2-m temperatures. The seasonal cycle provides an overall assessment of the temperature pattern for the entire 6-month period and is used to determine low-frequency changes in variability due to each forcing. For each of the five configurations, we quantify the strength of the seasonal cycle based on the standard deviation of the daily mean temperatures across all 100 years of the model simulations; hereinafter this quantity is referred to as seasonal cycle and is computed at each grid point. The seasonal-cycle parameters are computed as follows:

$$\overline{T}(d) = \frac{\sum_{d=1}^{100} T(d,y)}{100}, \tag{1}$$

$$\overline{\overline{T}} = \frac{\sum_{d=1}^{181} \overline{T}(d)}{181}, \quad \text{and} \tag{2}$$

$$T_{\text{std\_sc}} = \left\{ \frac{\sum_{d=1}^{181} [\overline{T}(d) - \overline{\overline{T}}]^2}{180} \right\}^{1/2}. \quad (3)$$

In the above equations (and all that follow), the index d denotes the day and ranges in value from 1 to 181 (corresponding to 1 November–30 April of the following year, with no leap days). The index y corresponds to the year of the model run (for the AMIP simulations this would be 1–100). The variable $\overline{T}(d)$ represents the daily mean value of temperature [Eq. (1)], and $\overline{\overline{T}}$ denotes the seasonal mean value of the daily mean values [Eq. (2)]. Here, $T_{\text{std\_sc}}(y)$ is the standard deviation of $\overline{T}(d)$ and represents the strength of the seasonal cycle [Eq. (3)]. An increase in $T_{\text{std\_sc}}$ would represent a more pronounced seasonal cycle—for example, warming during the early months and cooling in the middle period, creating a larger range in the temperature values over the entire season. Conversely a decrease in $T_{\text{std\_sc}}$ would signify a dampening of the seasonal cycle or a smaller range in seasonal temperatures.

Because the seasonal-cycle variability will not provide any information regarding variability at higher frequencies, we then assess the variability of temperature anomalies within a season, which removes the low-frequency seasonal cycle, leaving the intraseasonal anomalies. In this part, we subtract the daily temperature climatology calculated in Eq. (1) from the raw temperatures and compute the standard deviation of the daily anomalies within a season. This yields an analysis of temperature variability independent of the seasonal cycle. The computation is outlined below:

$$T_{\text{anom}}(d, y) = T(d, y) - \overline{T}(d), \quad (4)$$

where $T_{\text{anom}}(d, y)$ is the total daily anomaly that results from removing the daily temperature climatology. Following removal of the climatology, the process for quantifying variability within a season is the same as that of quantifying the strength of the seasonal cycle:

$$\overline{T_{\text{anom}}}(y) = \frac{\sum_{d=1}^{181} T_{\text{anom}}(d, y)}{181} \quad \text{and} \quad (5)$$

$$T_{\text{std\_ia}}(y) = \left\{ \frac{\sum_{d=1}^{181} [T_{\text{anom}}(d, y) - \overline{T_{\text{anom}}}(y)]^2}{180} \right\}^{1/2}, \quad (6)$$

where $\overline{T_{\text{anom}}}(y)$ is the 6-month mean value of the temperature anomalies for each year, representing interannual variations of the 6-month mean, and $T_{\text{std\_ia}}(y)$ is the "intraseasonal-anom" temperature standard deviation calculated each year. A two-tailed t test was performed comparing the 100 combinations of 8190ALL with the other configurations to determine significance of the differences between the standard deviations in alternate configurations and the control; 95% is chosen as the confidence interval.

The above analyses are repeated with CFSR data that are grouped into two 10-yr periods, 1981–90 and 2005–14, to match those of the boundary conditions in the model simulations (data from November 1981–April 1982 through November 1990–April 1991 are used to represent 1981–90, and data from November 2005–April 2006 through November 2014–April 2015 are used to represent 2005–14). Thus for the CFSR, we have 10 samples from November to April under similar forcings as opposed to 100 for the model simulations. Like for the model simulations, seasonal-cycle and intraseasonal-anom standard deviations are computed following the above equations (except with 10 years instead of 100, making the maximum value of y equal to 10). For intraseasonal-anom, the mean for the 1981–90 period is removed from the 1981–90 dataset, and the mean for the 2005–14 period is removed from the 2005–14 dataset. Treating the periods separately and using two sets of means (rather than removing the same mean from both datasets) is more representative of the analysis done with the model simulations. Like the model simulations, a significance test is also performed, but only with 10 samples as opposed to 100.

Area-weighted mean temperatures and anomalies (with seasonal cycles removed) are computed in the boxed regions that represent the greatest changes in standard deviations in CFSR and the model simulations. These boxes are defined as Eurasia (50°–70°N, 60°–120°E) and North America (50°–70°N, 60°–120°W) and are shown in Fig. 1 and all subsequent spatial maps. Other regions were tested (not shown), and it was found that these particular regions produced the most coherent results. For each box, we compute the average 2-m temperature anomalies to select the top 10% warmest and coldest extremes (defined as the means of the coldest and warmest 18 days of the total 181-day period).

We demonstrate the impact that changes in meridional winds and the temperature gradient have on temperature extremes, as sea ice loss strongly affects the meridional temperature gradient, which may also modulate the temperature extremes. The contribution of the meridional temperature advection to temperature tendency is

$$\frac{dT}{dt}(d, y) = -v(d, y) \times \frac{dT}{dY}(d, y). \quad (7)$$

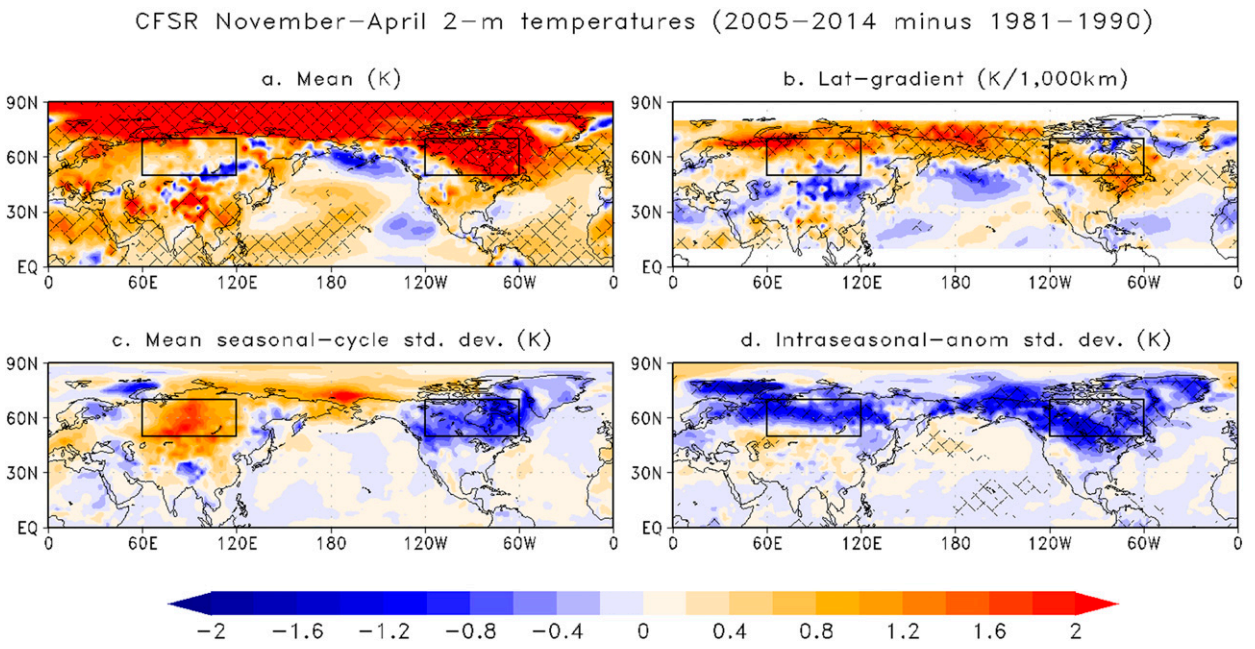

FIG. 1. The 2-m temperature differences in CFSR from 1 Nov through 30 Apr of the following year (2005–14 minus 1981–90): (a) mean difference (K), (b) latitudinal gradient mean difference (dT/dy; K per 1000 km), and mean (c) seasonal-cycle ($T_{\text{std\_sc}}$; K) and (d) intraseasonal-anom ($T_{\text{std\_ia}}$; K) standard deviation difference. Hatching in (a), (b), and (d) represents statistical significance at 95% confidence.

For simplicity, hereinafter we will refer to the resultant dT/dt term (which represents the meridional temperature advection) as Adv_m; T is the temperature, v is the meridional wind component, and y represents the geographic distance in the latitudinal direction. The latitudinal temperature gradient is computed using central finite differencing with a grid spacing of 20° latitude, equal to the width of the domains being analyzed in this study. As in the previous equations, d and y denote day and year, respectively, for each model configuration or CFSR data. Using Eq. (7), a simple argument can be made that under the same-magnitude northerly winds (negative v), and a weaker north–south temperature gradient (positive dT/dy), the Adv_m term would increase (become less negative). The opposite would be true with southerly winds; that is, the advection term would become less positive. This result would argue the case for smaller magnitudes of warm and cold extremes as associated temperature advection would presumably be weaker.

We compute the subseasonal meridional temperature advection standard deviation ($\text{Adv}_{m\_\text{std}}$) to illustrate the variability within each 6-month season:

$$\overline{\text{Adv}_m}(y) = \frac{\sum_{d=1}^{181} \text{Adv}_m(d,y)}{181} \quad \text{and} \tag{8}$$

$$\text{Adv}_{m\_\text{std}}(y) = \left\{ \frac{\sum_{d=1}^{181} \left[\text{Adv}_m(d,y) - \overline{\text{Adv}_m}(y)\right]^2}{180} \right\}^{1/2}. \tag{9}$$

In Eqs. (8) and (9), $\overline{\text{Adv}_m}$ denotes the 6-month mean of meridional temperature advection computed for each November–April period in the AMIP simulations and CFSR.

3. Results

a. Analysis of subseasonal 2-m temperature

Temperature differences in CFSR between 1981–90 and 2005–14 show warming across much of the Northern Hemisphere (Fig. 1a), with the largest and statistically significant increases in the Arctic (average of 2.3 K for all points north of 70°N). These large changes in the Arctic extend southward into the North America region (mean increase of 2.1 K) but are more moderate over Eurasia (mean increase of 0.35 K). Mean temperature gradients are likewise affected (Fig. 1b), with mean increases of 0.62 and 0.60 K per 1000 km for Eurasia and North America, respectively. These increases represent a weakening of the amplitude of the negative north–south gradient (warm in the south but less cold in the

north). The seasonal-cycle standard deviation (Fig. 1c) increases by 1.11 K in Eurasia and decreases by 0.71 K over North America. Removal of 6-month seasonal anomalies (Fig. 1d) produces reductions in standard deviations of daily temperature anomalies in both regions with mean changes of −0.51 and −0.79 K for Eurasia and North America, respectively.

Figure 2 shows the 2-m mean temperature and temperature gradient changes in the model simulations. Simulations that have reduced sea ice (0514ALL and 0514ICE) have the largest amount of warming in the Arctic, similar to that seen in CFSR. Mean 2-m temperature change for 0514ALL and 0514ICE relative to 8190ALL for all points north of 70°N is 3.1 and 2.5 K, respectively, with much smaller amounts (less than 0.4 K) for the other simulations. Mean temperature changes in the Eurasia and North America domains in 0514ALL are 0.82 and 0.89 K, respectively, and for 0514ICE are 0.48 and 0.76 K, respectively. The temperature changes are significant throughout most of the Northern Hemisphere for 0514ALL and 0514SST, but limited to the higher latitudes for 0514ICE. Significance is not widespread in $0514CO_2$. The gradient differences in the AMIP simulations are most comparable to CFSR in 0514ALL (Fig. 2e) and 0514ICE (Fig. 2g), with minimal changes in 0514SST (Fig. 2e) and $0514CO_2$ (Fig. 2h).

Model simulated seasonal-cycle and intraseasonal-anom standard deviation differences are shown in Fig. 3. Only modest changes in the seasonal-cycle standard deviations are found in the model simulations, with 0514ICE showing the greatest increases (decreases) in standard deviation over Eurasia (North America), consistent with the changes in CFSR. Significant decreases were found in 0514ALL and 0514ICE (runs in which sea ice was decreased) for intraseasonal-anom. For Eurasia the changes were −0.26 and −0.30 K for 0514ALL and 0514ICE, respectively, and for North America the differences were −0.36 and −0.33 K for 0514ALL and 0514ICE, respectively.

The mean seasonal cycles of 2-m temperature differences from November to April are shown in Fig. 4a (Eurasia) and Fig. 4b (North America) for CFSR (2005–14 minus 1981–90) and the AMIP simulations (relative to 8190ALL). We use a 30-day running average to further smooth the differences. A mean decrease of −1.1 K over Eurasia is found from 15 January to 15 February in CFSR. However, this decrease is not statistically significant. Significant increases in 2-m temperature do exist in CFSR after 15 March. The decrease in midwinter temperatures in CFSR over Eurasia, in addition to the increase in spring temperatures, would explain the higher standard deviations seen in the seasonal-cycle standard deviations in Fig. 1c as a result of a stronger seasonal cycle, and the increase in midwinter temperatures over North America would explain the decrease in standard deviations in Fig. 1d due to a dampened seasonal cycle.

The AMIP simulations are more modest with temperature changes; however, because of the larger sample, they have a higher significance, particularly for the simulations with reduction in sea ice. Over Eurasia, significant temperature increases are found in 0514ALL, 0514SST, and 0514ICE early in the period (15 November–15 December) but not in the remainder of the period (the exception is a small amount of significance found in 0514ALL around 1 February). The fact that the model simulations do not show the winter cooling over Eurasia, and the subsequent increased standard deviation that is present in CFSR, suggest that the temperature changes in CFSR might be more related to internal variability (also see the analysis below), agreeing with the results of Collow et al. (2018). Conversely, over North America, there are significant temperature increases found in 0514ALL and 0514ICE corresponding to the changes in CFSR, although they are much smaller in magnitude (0.85 and 0.74 K, respectively), which can likely be attributed to the smaller sample size (10 vs 100 model years).

Next, we test whether random 10-yr model sample differences can capture the pattern seen in the CFSR difference. This is done both to assess model fidelity, in terms of whether the model is capable of representing the observed pattern, and to provide an assessment of internal variability. Using the smoothed time series data discussed above, we took the mean of 10 random model years and took the difference relative to the mean of 10 random samples of 8190ALL. We repeated this 5000 times for both domains, and for each instance computed the root-mean-square error (RMSE) with respect to the CFSR differences in Figs. 4a and 4b. Figures 4c and 4d show the best 10-yr difference (lowest RMSE) for Eurasia and North America, respectively. All of the model simulations are capable of capturing the observed cooling over Eurasia and the warming over North America. Figures 4e and 4f show the distribution of RMSE as a percentage of the 5000 samples. For Eurasia (Fig. 4e), the distribution is fairly uniform, with 0514ALL being a bit on the warmer side of the other simulations. This would argue that the observed cooling over Eurasia is more likely a function of internal variability. For North America (Fig. 4f), it is clear that simulations that reduce sea ice (0514ALL and 0514ICE) are more capable of reproducing the observed increase in temperature as the RMSE distributions of those model configurations are both shifted in the direction of lower RMSE values relative to 0514SST and 0514CO2.

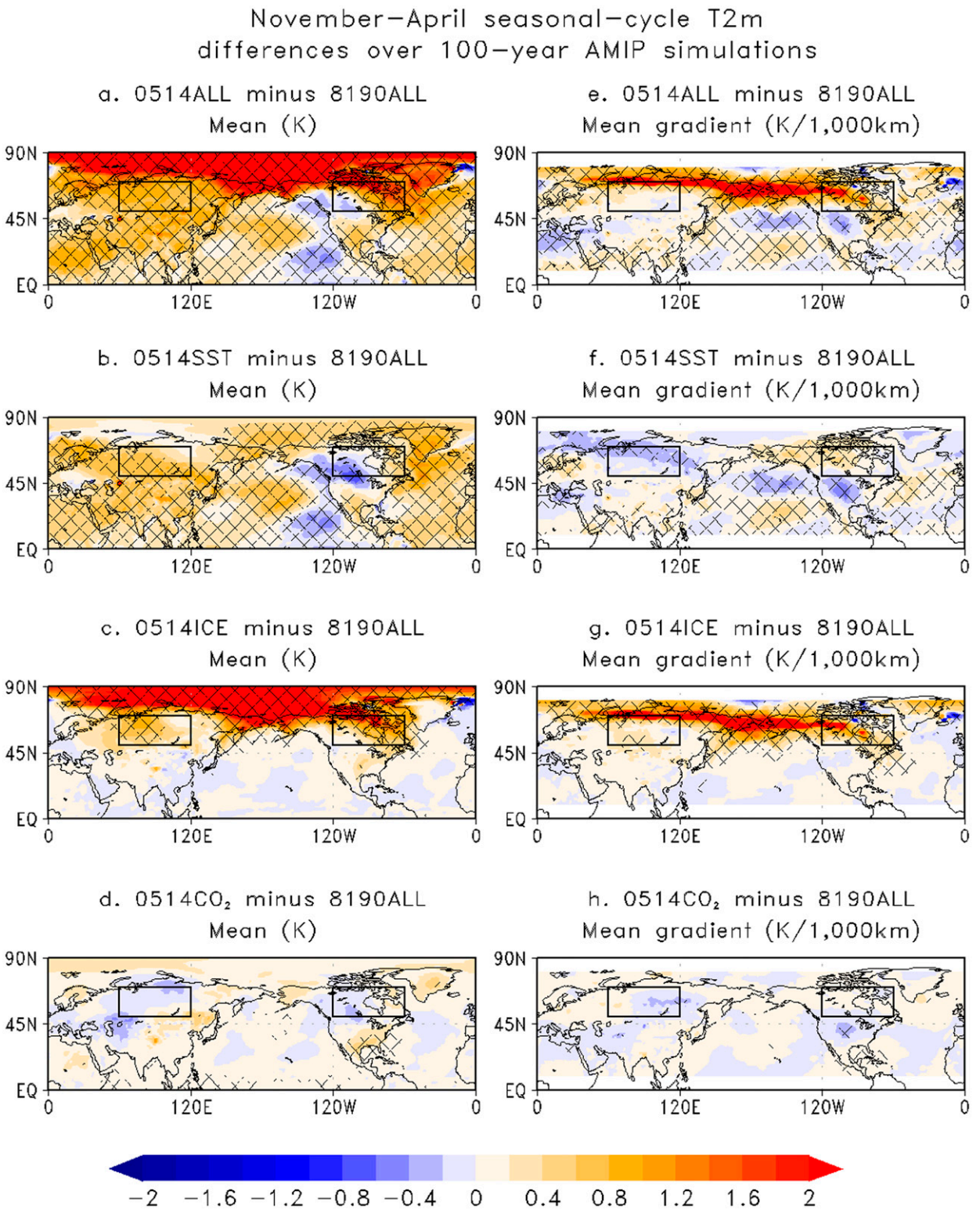

FIG. 2. The 2-m temperature (left) mean (K) and (right) latitudinal mean gradient (dT/dy; K per 1000 km), differences from CFSv2 AMIP simulations: (a),(e) 0514ALL minus 8190ALL; (b),(f) 0514SST minus 8190ALL; (c),(g) 0514ICE minus 8190ALL; and (d),(h) 0514CO_2 minus 8190ALL. Hatching represents statistical significance at 95% confidence.

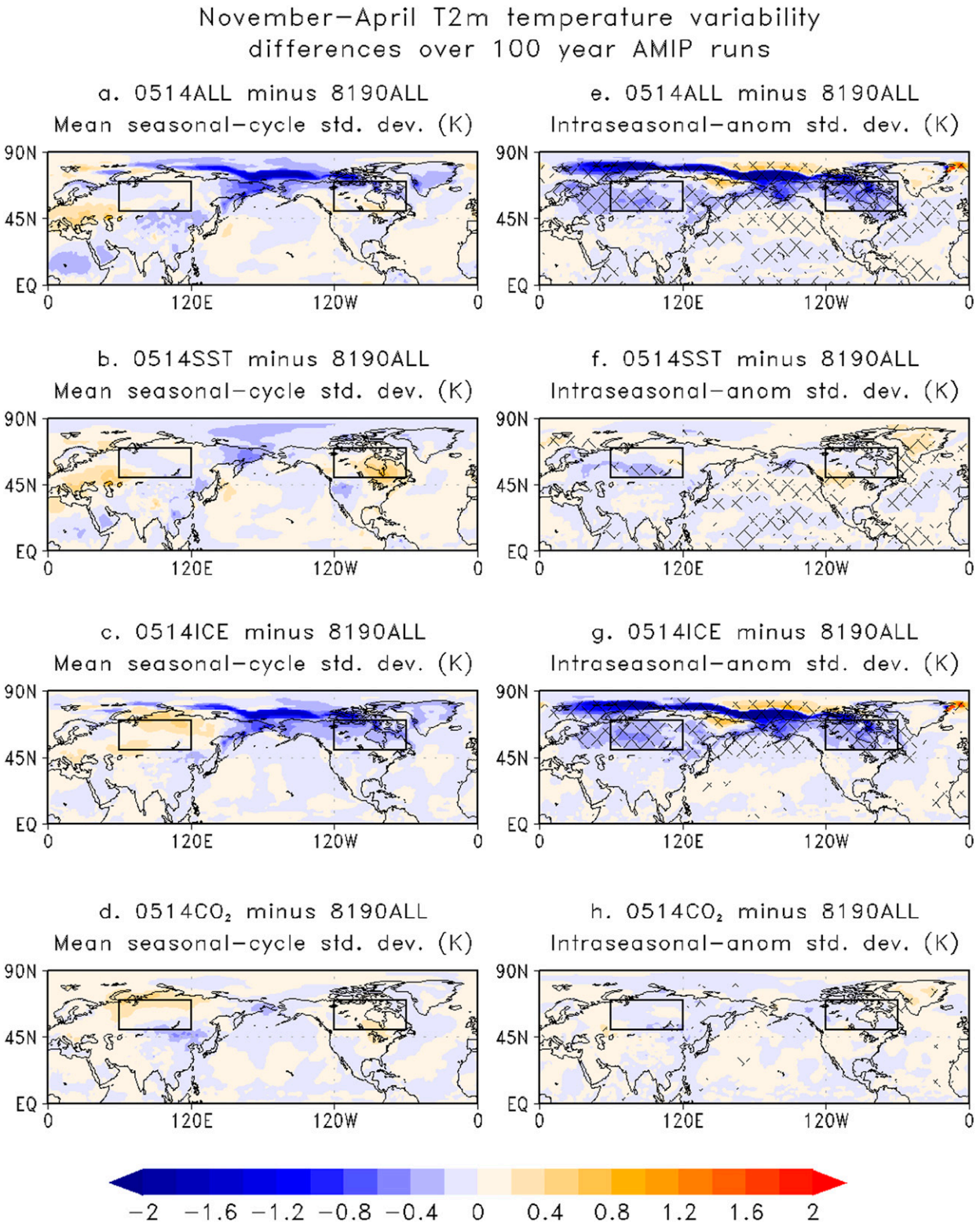

FIG. 3. As in Fig. 2, but for (left) seasonal-cycle (T_{std_sc}; K) and (right) intraseasonal-anom (T_{std_ia}; K) standard deviation differences. Hatching in (e)–(h) represents statistical significance at 95% confidence.

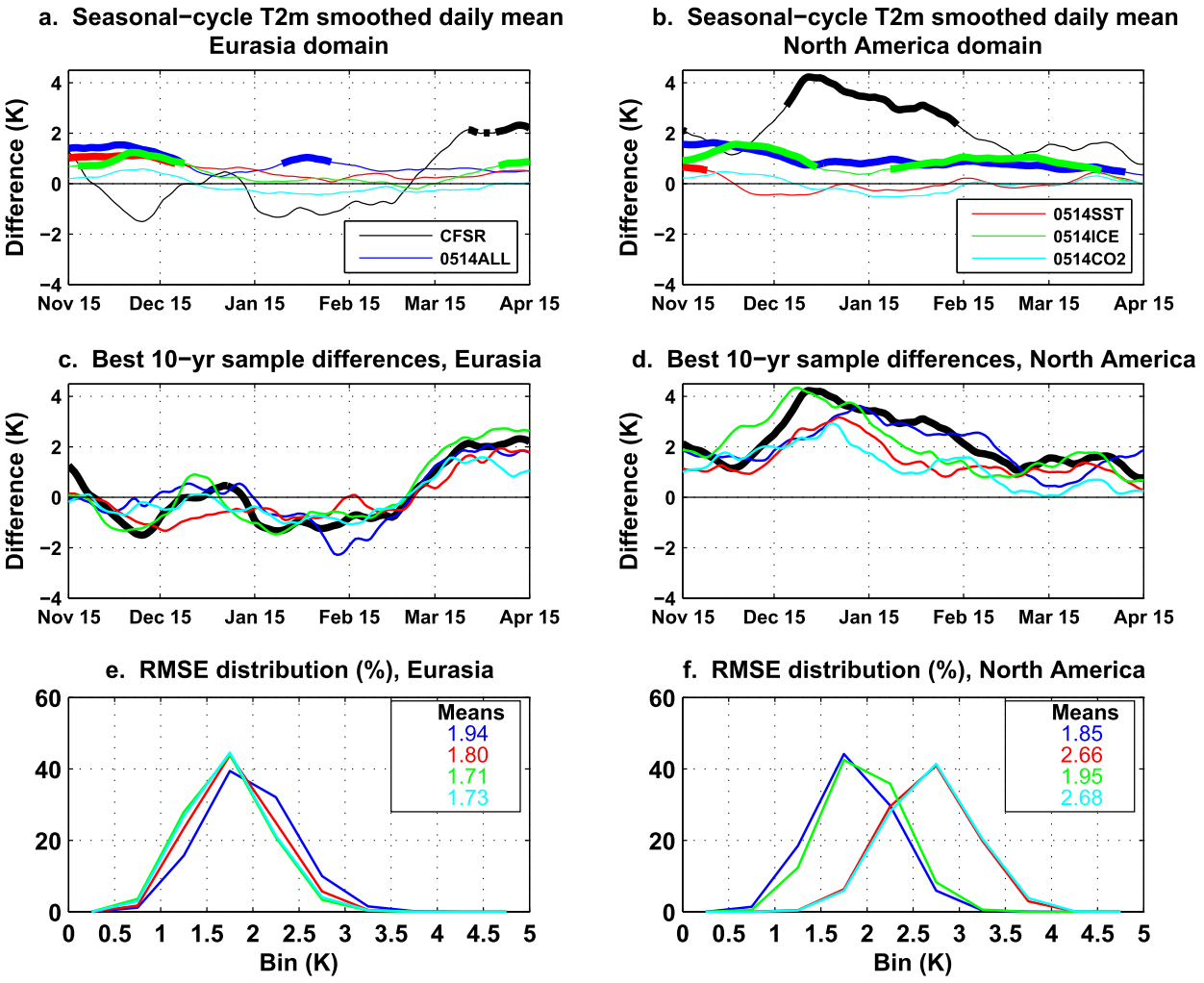

FIG. 4. (a),(b) seasonal cycle of 2-m temperature differences [the thick lines denote statistical significance with respect to 1981–90 (CFSR) and 8190ALL (AMIP simulations)]; (c),(d) best 10-yr mean model differences with respect to 8190ALL determined by finding the lowest RMSE of 5000 random samples relative to the CFSR difference; and (e),(f) RMSE distribution for the (left) Eurasia and (right) North America domains.

Changes in the amplitude of temperature anomaly extremes are investigated in Fig. 5a (cold extremes) and Fig. 5b (warm extremes). We note that in model simulations this analysis is relative to its own climatology, while in observations it is relative to its own 10-yr base period. The extreme values in each 6-month season are determined based on the top and bottom 10% of the temperature anomaly distribution from each season. The lowest 10% of temperature anomaly values for each of the 100 seasons (AMIP) or 10 seasons (CFSR) are averaged together to determine the mean temperature anomaly for cold extremes, and the process is repeated with the top 10% of values for the warm extreme anomaly mean. An average of all cold and warm extreme anomalies is taken over all years and is shown in Figs. 5a and 5b. There is a significant reduction in cold temperature anomaly extremes for the Eurasia domain in 0514ICE, by a magnitude of 0.60 K, suggesting that in the new mean state that results from sea ice loss the coldest temperatures deviate less from the mean than they did in the mean state for 8190ALL. For 0514ALL, the cold anomaly extreme change was 0.46 K but was not significant. Over North America, the amplitude of reduction in cold extreme anomalies was 0.57 and 0.49 K, and both were significant for 0514ALL and 0514ICE, respectively. CFSR also showed warming of cold extreme anomalies that were higher in magnitude than the model but were not significant (increases by 0.88 and 0.66 K for the Eurasia and North America domains, respectively). Warm extremes show the same relationship

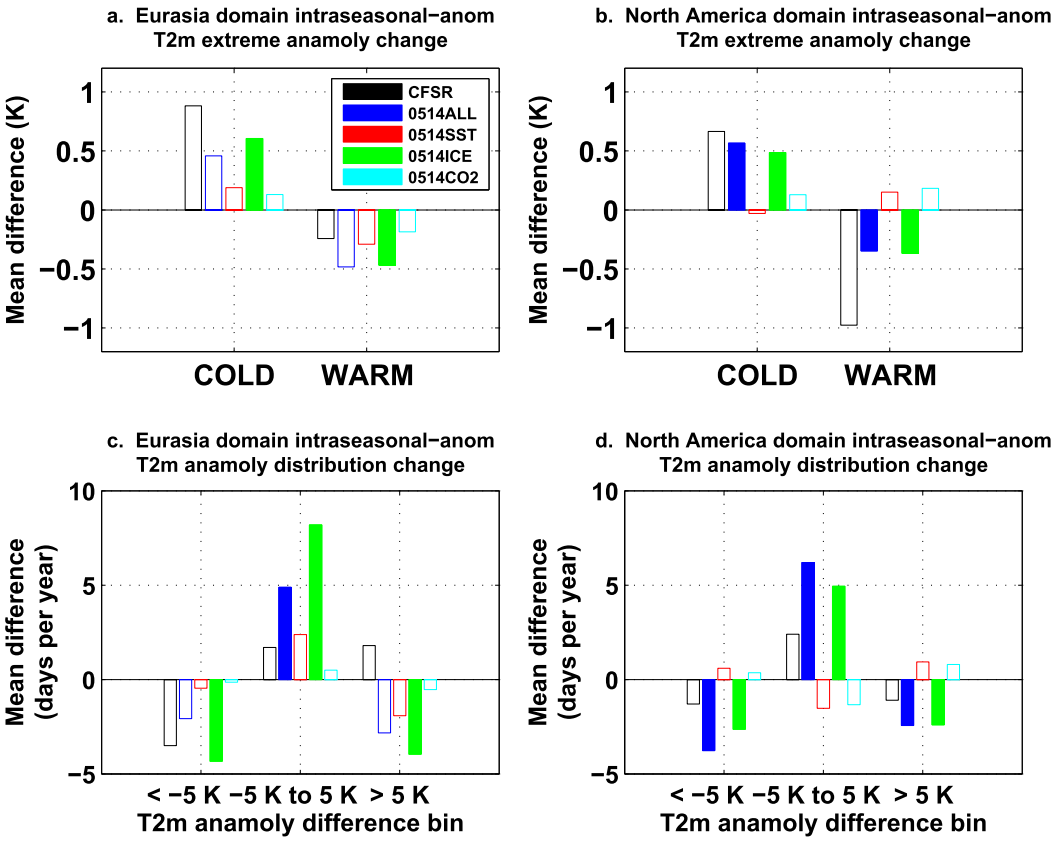

FIG. 5. (a),(b) Mean change in the bottom 10% ("COLD") and top 10% ("WARM") temperature extremes (K) from intraseasonal-anom computed for each 181-day period (for CFSR the differences are 2005–14 minus 1981–90; for the AMIP simulations the differences are relative to 8190ALL) and (c),(d) mean change in the temperature anomaly distribution (days per year) for the (left) Eurasia and (right) North America domains. Shaded bars represent statistical significance at 95% confidence.

with the extremes deviating less from the new mean state. Changes of −0.48 and −0.35 K are found in 0514ALL for the Eurasia and North America domains, respectively (significant over the North America domain); for 0514ICE, the changes are −0.47 and −0.37 K, respectively, for Eurasia and North America (results from both domains are statistically significant). In the Eurasia domain the change in magnitude in CFSR is −0.24 K; for the North America domain the change is −0.98 K. Neither of these changes in CFSR is significant.

Figures 5c and 5d illustrate the change in the distribution of intraseasonal temperature anomalies by assigning three possible bins (<−5, −5 to 5, and >5 K), and determining the average frequency of occurrence over 100 yr for the AMIP simulations and 10 yr for CFSR. The values plotted are differences from the distribution relative to 8190ALL or the CFSR 1981–90 period. It is evident that for both the Eurasia and North America domains there are decreases in the occurrences of both warm and cold temperature extremes (defined here as temperature anomalies colder than 5 K for cold extremes and warmer than 5 K for warm extremes, with anomalies in between denoted as neutral). Over the Eurasia domain, changes in the frequency of occurrences of extremes for CFSR are −3.5 days yr^{-1} for cold, 1.7 days yr^{-1} for neutral, and 1.8 days yr^{-1} for warm. For North America, these values are −1.3, 2.4, and −1.1 days yr^{-1} for cold, neutral, and warm, respectively. Patterns were more robust for the model simulations, likely because of the larger sample size. The results for simulations that reduce sea ice are the most noteworthy. Changes in extremes over the Eurasia domain were −2.1, 4.9, and −2.8 for 0514ALL for cold, neutral, and warm, respectively; for 0514ICE they were −4.3, 8.2, and −4 days yr^{-1} for cold, neutral, and warm extremes, respectively. Over the North America domain, a similar pattern is seen, with changes for 0514ALL being −3.8 days yr^{-1} for cold extremes, 6.2 for neutral, and −2.4 for warm extremes. For 0514ICE, the values

were −2.6, 4.9, and −2.4 days yr^{-1} for cold, neutral, and warm extremes, respectively.

b. *Proposed mechanism for decrease in the magnitude of extremes*

Next, we investigate a potential mechanism for the decrease in magnitudes of both warm and cold temperature extremes. First, we examine changes in the mean and the variability of the meridional wind, which is shown in Fig. 6. In CFSR, significant increases in mean southerly winds are noted in the vicinity of the Barents and Kara Seas (Fig. 6a), which may signify an increase in the strength of the Siberian high, although significant changes in the wind over Eurasia were not observed. Cohen et al. (2001) established that the Siberian high was a dominant source of climate variability over Eurasia during the winter. Unlike in other studies that showed that this anticyclonic flow occurs more frequently (Honda et al. 2009; Zhang et al. 2012; Zappa et al. 2018) resulting in more frequent cold extremes, in our model simulations we did not find significant changes in the surface meridional wind, in terms of both the mean and the variability over the Eurasia and North America domains, and show only significant changes locally where the sea ice decreases took place (Figs. 6b,d,g,i). The changes in wind magnitude at the middle and lower latitudes are more attributed to changes in SST and not to changes in sea ice (Fig. 6c).

Figure 7 examines the Adv_m and Adv_{m_std} terms calculated in Eqs. (8) and (9), respectively, for CFSR, and the AMIP simulations. In terms of the mean meridional temperature advection, significant changes are sparse in CFSR (Fig. 7a) but more apparent in AMIP simulations that reduce sea ice over the North Pacific (Figs. 7a,d). SST changes also result in some positive increases in advection in this region, but are not as robust as with the sea ice changes. Of note, these positive changes are reductions in negative meridional temperature advection. CFSR shows a fairly large decrease in the variability of meridional temperature advection across the northern midlatitudes in the 2015–14 period relative to the 1981–90 period, with some areas significant (Fig. 7e). Decreases for Eurasia and North America were −0.18 and −0.12 K day^{-1}, respectively. The AMIP simulations where sea ice was reduced were most robust in highlighting the changes over North America, −0.13 K day^{-1} for both 0514ALL (Fig. 7f) and 0514ICE (Fig. 7i). For Eurasia, changes were more modest but there were some areas of significant reductions in 0514ICE. Area mean values were −0.04 and −0.05 K day^{-1} for 0514ALL and 0514ICE, respectively. Both CFSR and the AMIP solutions showed very large decreases over the North Pacific and in the vicinity of Alaska. As with the winds, changes in the meridional temperature advection variability in the middle and lower latitudes could only be duplicated in 0514SST (Fig. 7h). Changes in zonal temperature advection were also investigated (not shown) and were found to be less robust than in the meridional component. Tables 2 and 3 show the area mean values for meridional temperature advection standard deviation and intraseasonal-anom 2-m temperature standard deviation for the Eurasia and North America domains, respectively. We conclude that the reduced meridional temperature gradient that results from sea ice loss leads to a decrease in the variability of meridional temperature advection (3%–4% decrease over Eurasia in the AMIP runs that reduce sea ice, and 7%–8% decrease over North America), and therefore smaller temperature deviations from the mean state, reducing the intraseasonal variability. This mechanism was most robust over North America, but significant changes were apparent over Eurasia as well despite the small decreases.

4. Discussion and conclusions

Results of this study build on our previous work highlighting the role of sea ice loss in northern midlatitude surface temperature variability. The experiment design allowed us to isolate the impacts of changes in SST, sea ice, and CO_2 concentration on subseasonal 2-m temperature variability in the November–April period. In the CFSR reanalysis, seasonal-cycle November–April temperature variability increased over Eurasia along with winter cooling in the recent decade, similar with results in Cohen (2016). However, none of the 100-yr means of the model simulations exhibited the cooling or the increase in temperature variability shown in CFSR, indicating that the recent cooling over Eurasia may be more related to internal variability of the climate system rather than to any external forcing (McCusker et al. 2016; Sun et al. 2016; Collow et al. 2018). However, the AMIP simulations that include the reduced Arctic sea ice best represent the decrease in intraseasonal-anom standard deviations as seen in CFSR over both Eurasia and North America, but with a smaller magnitude. The larger amplitude in reanalysis data than in the model simulations suggests that the observed trend may have been amplified by internal variability. Nonetheless, results show that Arctic sea ice loss plays some role in modifying the nonlocal climate. Several studies (Screen et al. 2014, 2015; Blackport and Kushner 2016; Sun et al. 2016) conclude a decrease in the variability of surface temperatures in the northern midlatitudes due to the decreased temperature gradients imposed by sea ice loss. This study takes the analysis a step further by offering insight into how reduced gradients play a role in

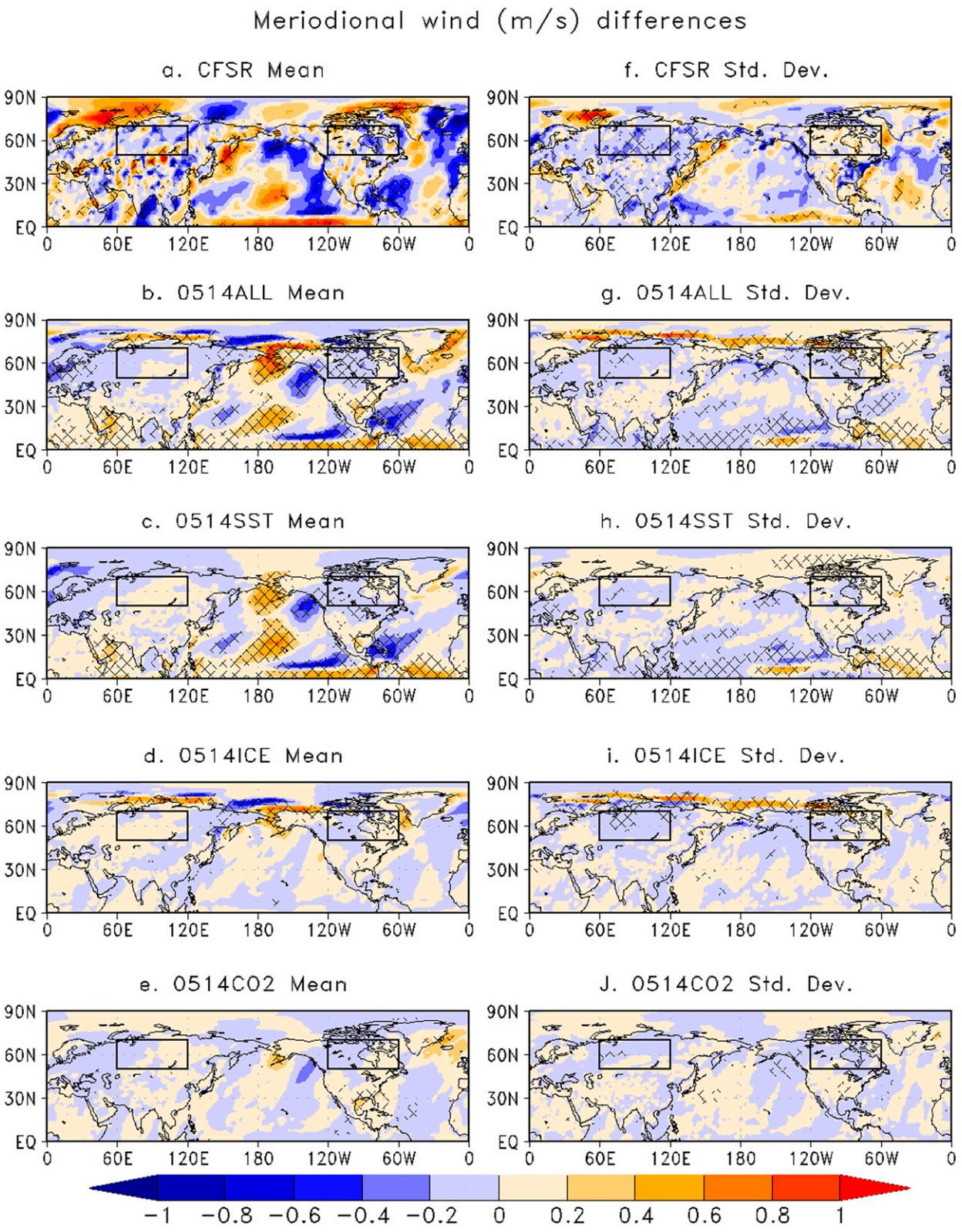

FIG. 6. Differences in the (left) mean and (right) subseasonal standard deviation of the meridional wind speed (m s^{-1}) for (a),(f) CFSR; (b),(g) 0514ALL; (c),(h) 0514SST; (d),(i) 0514ICE; and (e),(j) 0514CO2 (for CFSR the differences are 2005–14 minus 1981–90; for the AMIP simulations the differences are relative to 8190ALL). Hatching denotes statistical significance at 95% confidence.

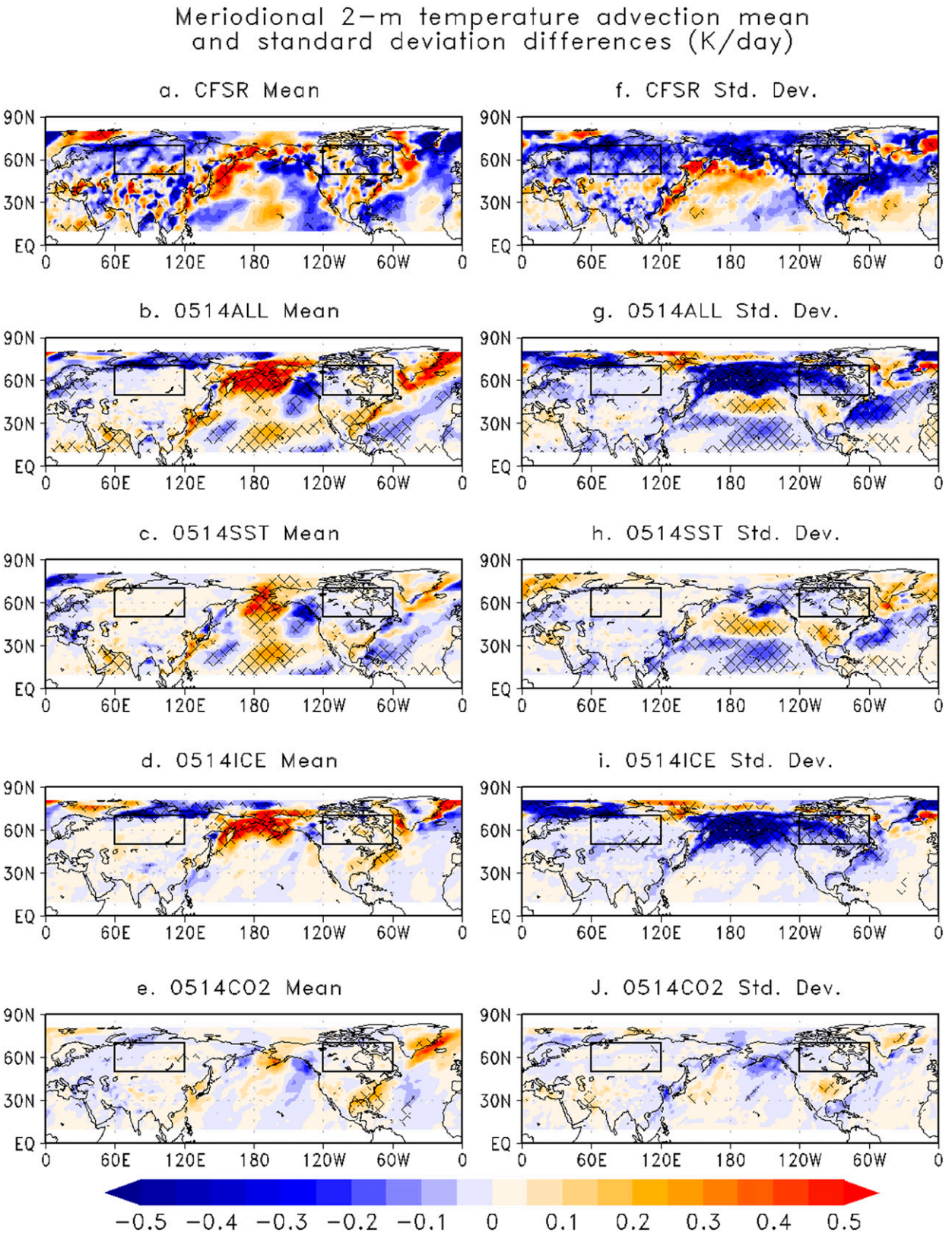

FIG. 7. Differences in the subseasonal (left) mean and (right) standard deviation of meridional temperature advection (K day^{-1}) for (a),(f) CFSR; (b),(f) 0514ALL; (c),(g) 0514SST; (d),(h) 0514ICE; and (e),(i) 0514CO2 (for CFSR the differences are 2005–14 minus 1981–90; for the AMIP simulations the differences are relative to 8190ALL). Hatching denotes statistical significance at 95% confidence.

TABLE 2. Meridional temperature advection (K day^{-1}) and intraseasonal-anom standard deviation (K) area mean values and differences over the Eurasia domain. For CFSR the difference is the 2005–14 period relative to the 1981–90 period, and for the model simulations the differences are relative to 8190ALL. Boldface type denotes that the differences are significant at the 95% confidence interval.

	Meridional temperature advection std dev area mean	Meridional temperature advection std dev diff	Meridional temperature advection std dev % diff	Intraseasonal-anom std dev area mean	Intraseasonal-anom std dev diff	Intraseasonal-anom std dev % diff
CFSR						
1981–90	1.23			6.46		
2005–14	1.05	**−0.18**	−14.63	5.95	**−0.51**	−7.90
AMIP						
8190ALL	1.26			7.19		
0514ALL	1.22	**−0.04**	−3.17	6.93	**−0.26**	−3.62
0514SST	1.26	0.00	0.00	7.09	−0.10	−1.39
0514ICE	1.21	**−0.05**	−3.97	6.89	**−0.30**	−4.17
0514CO2	1.26	0.00	0.00	7.13	−0.06	−0.83

temperature advection over two key regions, and how changes in the variability of temperature advection impact the frequency of temperature extremes.

The model simulations with changed sea ice have the greatest amount of surface warming in the Arctic with less in the lower latitudes. This reduces the north–south temperature gradient as pointed out in previous studies (e.g., Francis and Vavrus 2012). However, we did not see substantial changes in temperatures above the surface [see Collow et al.'s (2018) Fig. 5 as a reference], indicating that the surface temperature changes alone are the primary driver for the changes in variability. Our results are more in line with previous work by Holmes et al. (2016) that showed that changes in the mean state temperature gradients account for the majority of the changes in temperature variability. Schneider et al. (2015) explain that Arctic amplification of global warming leads to less frequent cold outbreaks than just a warmer climate itself, meaning that again the decreased gradients play a key role. Screen et al. (2014) also established a reduction in temperature variability in the northern midlatitudes due to a smaller difference in temperature advection between northerly and southerly winds.

Our study found that the variability of the subseasonal temperature advection decreased owing to a decrease in both anomalous warm and cold extremes, thus reducing 2-m temperature variability. We did not note any significant changes in winds (zonal or meridional) remotely due to sea ice loss. Blackport and Kushner (2016) showed only very weak decreases in Arctic upper-level zonal winds and concluded that additional work is needed to determine whether or not those changes are the result of sea ice loss, or an overall consequence of mean global warming. As in our study, their mean temperature changes were confined to the lower troposphere of the high latitudes. Although we only focused on surface winds (10 m), we conclude that changes are more likely the result of SST increases and not sea ice loss. Since the winds are generally unchanged, we conclude that the reduced temperature gradient is responsible for the reduction in surface temperature variability and does so through weaker warm and cold temperature advection, seen through the reduced standard deviations.

The most robust results occurred over North America, which had more warming and temperature gradient

TABLE 3. As in Table 2, but for the North America domain.

		Meridional temperature advection std dev area mean	Meridional temperature advection std dev diff	Meridional temperature advection std dev % diff	Intraseasonal-anom std dev area mean	Intraseasonal-anom std dev diff
CFSR						
1981–90	1.85			6.16		
2005–14	1.73	**−0.12**	−6.49	5.37	**−0.79**	−12.82
AMIP						
8190ALL	1.73			5.88		
0514ALL	1.59	**−0.14**	−8.09	5.52	**−0.36**	−6.12
0514SST	1.72	−0.01	−0.58	5.89	0.01	0.17
0514ICE	1.60	**−0.13**	−7.51	5.55	**−0.33**	−5.61
0514CO2	1.72	−0.01	−0.58	5.86	−0.02	−0.34

reduction within the domain than over Eurasia (Fig. 2), and the changes could be better attributed to the sea ice loss rather than internal variability (Fig. 4). Other mechanisms are likely in place and require further testing (i.e., changes in surface properties, cloud cover, vertical temperature profiles), in addition to investigating localized changes in temperature variability due to sea ice loss in a specific region at a certain time within the 6-month period (i.e., Hudson Bay). Our primary result regarding larger-scale changes in temperature variability agrees with several other published works and adds to the growing consensus that sea ice loss can only explain reductions in near-surface temperature variability over the northern midlatitudes.

In conclusion, answers to the questions posed in section 1 are as follows: 1) Mean seasonal-cycle differences in the AMIP runs are not substantial, but it is shown that, at times, all of the model simulations are capable of reproducing the seasonal-cycle differences from the two CFSR periods. AMIP simulations that reduce sea ice loss (0514ALL and 0514ICE) have the greatest reduction in 2-m temperature anomaly variability over the northern midlatitudes. The reduction in temperature anomaly variability is found to be significant and representative of a long-term pattern change as a result of sea ice conditions remaining at 2005–14 levels. 2) Sea ice loss reduces the temperature anomaly variability through decreasing the magnitude of both warm and cold extremes, confirming our hypothesis at the end of section 2. 3) While an exact pathway linking the sea ice loss with the temperature variability decrease is difficult to establish, it would appear that the reduced north–south temperature gradient works to reduce temperature extremes through reductions in the variability of meridional temperature advection.

Acknowledgments. This work is supported by the NOAA Climate Program Office Climate Variability and Predictability (CVP) Program. The authors thank Emerson LaJoie (CPC), Stephen Baxter (CPC), and three anonymous reviewers for their assessment of this paper.

REFERENCES

Barnes, E. A., 2013: Revisiting the evidence linking Arctic amplification to extreme weather in midlatitudes. *Geophys. Res. Lett.*, **40**, 4734–4739, https://doi.org/10.1002/grl.50880.

——, E. Dunn-Sigouin, G. Masato, and T. Woollings, 2014: Exploring recent trends in Northern Hemisphere blocking. *Geophys. Res. Lett.*, **41**, 638–644, https://doi.org/10.1002/2013GL058745.

Blackport, R., and P. J. Kushner, 2016: The transient and equilibrium climate response to rapid summertime sea ice loss in CCSM4. *J. Climate*, **29**, 401–417, https://doi.org/10.1175/JCLI-D-15-0284.1.

——, and ——, 2017: Isolating the atmospheric circulation response to Arctic sea ice loss in the coupled climate system. *J. Climate*, **30**, 2163–2185, https://doi.org/10.1175/JCLI-D-16-0257.1.

Cohen, J., 2016: An observational analysis: Tropical relative to Arctic influence on midlatitude weather in the era of Arctic amplification. *Geophys. Res. Lett.*, **43**, 5287–5294, https://doi.org/10.1002/2016GL069102.

——, K. Saito, and D. Entekhabi, 2001: The role of the Siberian high in Northern Hemisphere climate variability. *Geophys. Res. Lett.*, **28**, 299–302, https://doi.org/10.1029/2000GL011927.

——, J. C. Furtado, M. A. Barlow, V. A. Alexeev, and J. E. Cherry, 2012: Arctic warming, increasing snow cover and widespread boreal winter cooling. *Environ. Res. Lett.*, **7**, 014007, https://doi.org/10.1088/1748-9326/7/1/014007.

——, and Coauthors, 2014: Recent Arctic amplification and extreme mid-latitude weather. *Nat. Geosci.*, **7**, 627–637, https://doi.org/10.1038/ngeo2234.

Collow, T. W., W. Wang, and A. Kumar, 2018: Simulations of Eurasian winter temperature trends in coupled and uncoupled CFSv2. *Adv. Atmos. Sci.*, **35**, 14–26, https://doi.org/10.1007/s00376-017-6294-0.

Francis, J. A., and S. J. Vavrus, 2012: Evidence linking Arctic amplification to extreme weather in mid-latitudes. *Geophys. Res. Lett.*, **39**, L06801, https://doi.org/10.1029/2012GL051000.

——, and ——, 2015: Evidence for a wavier jet stream in response to rapid Arctic warming. *Environ. Res. Lett.*, **10**, 014005, https://doi.org/10.1088/1748-9326/10/1/014005.

Holmes, C. R., T. Woollings, E. Hawkins, and H. de Vries, 2016: Robust future changes in temperature variability under greenhouse gas forcing and the relationship with thermal advection. *J. Climate*, **29**, 2221–2236, https://doi.org/10.1175/JCLI-D-14-00735.1.

Honda, M., J. Inoue, and S. Yamane, 2009: Influence of low Arctic sea-ice minima on anomalously cold Eurasian winters. *Geophys. Res. Lett.*, **36**, L08707, https://doi.org/10.1029/2008GL037079.

Hurrell, J. W., J. J. Hack, D. Shea, J. M. Caron, and J. Rosinski, 2008: A new sea surface temperature and sea ice boundary dataset for the Community Atmosphere Model. *J. Climate*, **21**, 5145–5153, https://doi.org/10.1175/2008JCLI2292.1.

Inoue, J., M. E. Hori, and K. Takaya, 2012: The role of Barents Sea ice in the wintertime cyclone track and emergence of a warm-Arctic cold-Siberian anomaly. *J. Climate*, **25**, 2561–2568, https://doi.org/10.1175/JCLI-D-11-00449.1.

Kumar, A., and Coauthors, 2010: Contribution of sea ice loss to Arctic amplification. *Geophys. Res. Lett.*, **37**, L21701, https://doi.org/10.1029/2010GL045022.

LaJoie, E., and T. DelSole, 2016: Changes in internal variability due to anthropogenic forcing: A new field significance test. *J. Climate*, **29**, 5547–5560, https://doi.org/10.1175/JCLI-D-15-0718.1.

Liu, J. P., J. A. Curry, H. J. Wang, M. R. Song, and R. M. Horton, 2012: Impact of declining Arctic sea ice on winter snowfall. *Proc. Natl. Acad. Sci. USA*, **109**, 4074–4079, https://doi.org/10.1073/pnas.1114910109.

McCusker, K. E., J. C. Fyfe, and M. Sigmond, 2016: Twenty-five winters of unexpected Eurasian cooling unlikely due to Arctic sea-ice loss. *Nat. Geosci.*, **9**, 838–842, https://doi.org/10.1038/ngeo2820.

Moorthi, S., H.-L. Pan, and P. Caplan, 2001: Changes to the 2001 NCEP operational MRF/AVN global analysis/forecast

system. NOAA/National Centers for Environmental Prediction Tech. Bull. 484, 14 pp.

Nakamura, T., K. Yamazaki, K. Iwamoto, M. Honda, Y. Miyoshi, Y. Ogawa, and J. Ukita, 2015: A negative phase shift of the winter AO/NAO due to the recent Arctic sea-ice reduction in late autumn. *J. Geophys. Res. Atmos.*, **120**, 3209–3227, https://doi.org/10.1002/2014JD022848.

Ogawa, F., and Coauthors, 2018: Evaluating impacts of recent Arctic sea ice loss on the Northern Hemisphere winter climate change. *Geophys. Res. Lett.*, **45**, 3255–3263, https://doi.org/10.1002/2017GL076502.

Perlwitz, J., M. Hoerling, and R. Dole, 2015: Arctic tropospheric warming: Causes and linkages to lower latitudes. *J. Climate*, **28**, 2154–2167, https://doi.org/10.1175/JCLI-D-14-00095.1.

Saha, S., and Coauthors, 2010: The NCEP Climate Forecast System Reanalysis. *Bull. Amer. Meteor. Soc.*, **91**, 1015–1057, https://doi.org/10.1175/2010BAMS3001.1.

——, and Coauthors, 2014: The NCEP Climate Forecast System version 2. *J. Climate*, **27**, 2185–2208, https://doi.org/10.1175/JCLI-D-12-00823.1.

Schneider, T., T. Bischoff, and H. Plotka, 2015: Physics of changes in synoptic midlatitude temperature variability. *J. Climate*, **28**, 2312–2331, https://doi.org/10.1175/JCLI-D-14-00632.1.

Screen, J. A., 2014: Arctic amplification decreases temperature variance in northern mid- to high-latitudes. *Nat. Climate Change*, **4**, 577–582, https://doi.org/10.1038/nclimate2268.

——, 2017: The missing northern European winter cooling response to Arctic sea ice loss. *Nat. Commun.*, **8**, 14 603, https://doi.org/10.1038/ncomms14603.

——, and I. Simmonds, 2010: The central role of diminishing sea ice in recent Arctic temperature amplification. *Nature*, **464**, 1334–1337, https://doi.org/10.1038/nature09051.

——, and ——, 2013: Exploring links between Arctic amplification and mid-latitude weather. *Geophys. Res. Lett.*, **40**, 959–964, https://doi.org/10.1002/grl.50174.

——, C. Deser, I. Simmonds, and R. Tomas, 2014: Atmospheric impacts of Arctic sea-ice loss, 1979–2009: Separating forced change from atmospheric internal variability. *Climate Dyn.*, **43**, 333–344, https://doi.org/10.1007/s00382-013-1830-9.

——, ——, and L. Sun, 2015: Reduced risk of North American cold extremes due to continued Arctic sea ice loss. *Bull. Amer. Meteor. Soc.*, **96**, 1489–1503, https://doi.org/10.1175/BAMS-D-14-00185.1.

Sun, L. T., J. Perlwitz, and M. Hoerling, 2016: What caused the recent "warm Arctic, cold continents" trend pattern in winter temperatures? *Geophys. Res. Lett.*, **43**, 5345–5352, https://doi.org/10.1002/2016GL069024.

Tang, Q. H., X. J. Zhang, X. H. Yang, and J. A. Francis, 2013: Cold winter extremes in northern continents linked to Arctic sea ice loss. *Environ. Res. Lett.*, **8**, 014036, https://doi.org/10.1088/1748-9326/8/1/014036.

Zappa, G., F. Pithan, and T. G. Shepard, 2018: Multimodel evidence for an atmospheric circulation response to Arctic sea ice loss in the CMIP5 future projections. *Geophys. Res. Lett.*, **45**, 1011–1019, https://doi.org/10.1002/2017GL076096.

Zhang, X. D., C. H. Lu, and Z. Y. Guan, 2012: Weakened cyclones, intensified anticyclones and recent extreme cold winter weather events in Eurasia. *Environ. Res. Lett.*, **7**, 044044, https://doi.org/10.1088/1748-9326/7/4/044044.